SKIRTOR - database of modelled AGN dusty torus SEDs

Marko Stalevski[1,2]
[1] Astronomical Observatory, Volgina 7, 11000 Belgrade, Serbia
[2] Sterrenkundig Observatorium, Universiteit Gent, Krijgslaan 281-S9, Gent, 9000, Belgium
mstalevski@aob.rs
(Submitted on 17.08.2012; Accepted on 22.08.2012)

Abstract. We present a publicly available database of modeled SEDs of AGN dusty torus. The dusty torus was modeled as a 3D two-phase medium with high-density clumps and low-density medium filling the space between the clumps. This database contains a grid of models for different parameters of the torus. Also, for each two-phase model there are two corresponding models with the same global physical parameters: a clumps-only model and a model with a smooth dust distribution. Apart from the SEDs, images of torus for all points in the wavelength grid are also available. Here we provide a description of this database, with details on the structure of files and how to interpret them. These modeled SEDs can be used to interpret the observed infrared properties of AGN.
Key words: galaxies: active – galaxies: nuclei – galaxies: Seyfert – radiative transfer

Introduction

Active galactic nuclei (AGN) are powered by matter spiralling into a supermassive black hole in an accretion disk. The accretion disc is the source of the strong X-ray emission and UV/optical continuum. Superimposed on the continuum are the broad emission lines, coming from gaseous clouds moving at high velocities, the so-called broad-line region (BLR). This matter comes from a dusty torus which surrounds the central regions. The dusty torus has a major effect on the appearance of an AGN. The torus absorbs the incoming accretion disc radiation and re-emits it in the infrared domain. As a result, a mid-to far-infrared bump is observed in the spectral energy distribution (SED) of AGN. Furthermore, viewed edge-on, the dusty torus blocks the radiation coming from the accretion disc and BLR. In this case an UV/optical bump and broad emission lines are absent and the object appears as a type 2 AGN. In the case when the line of sight does not cross the dusty torus, both the accretion disc and BLR are exposed, giving rise to a strong UV/optical continuum and broad emission lines, and the object is classified as a type 1 active galaxy.

In order to prevent the dust grains from being destroyed by the hot surrounding gas, Krolik & Begelman (1988) suggested that the dust in the torus is organized in a large number of optically thick clumps. Wada & Norman (2002) (with a model update in Wada et al. 2009) performed a 3D hydrodynamical simulations of AGN tori, taking into account the self-gravity of the gas, the radiative cooling, and the heating due to supernovae. They found that such a turbulent medium would produce a multi-phase filamentary (sponge-like) structure, rather than isolated clumps.

We took a step further toward a more realistic model by treating the dusty torus as a two-phase medium, with high density clumps and a low density medium filling the space between them. We calculated SEDs and

images of the torus for a grid of parameters. For each two-phase model, our approach allows us to, generate a clumps-only model (with dust distributed in the clumps exclusively, without any dust between them) and a smooth model with the same global physical parameters. The details of our results and analysis of properties of the modeled dusty torus infrared emission can be found in Stalevski et al. (2012). The aim of this paper is to present SKIRTOR, publicly available database of model SEDs we calculated (`https://sites.google.com/site/skirtorus/`). These modeled SEDs can be used to interpret the observed infrared properties of AGN, such as, the intensity and shape of the silicate features, at 10 and 18 μm, which represent a unique window into the dust distribution and chemical composition even in relatively distant quasars. (Nikutta et al 2009; Stalevski et al. 2011, 2012). Recently, Roseboom et al. (2012) considered the optical to mid-IR properties of a sample of quasars selected from a combination of the WISE, UKIDSS and SDSS datasets. They estimated a number of quasar properties, including the IR SED shape characterised by the ratio of near-IR to total IR luminosity. They found that the near-IR to total IR luminosity ratios similar to that in their observed sample are easily achievable in our set of models.

1 Model

The detailed description of our model can be found in Stalevski et al. (2012). Here we will only provide a brief description of the most important properties of our model.

To obtain SEDs and images of dusty torus at different wavelength, we have used the radiative transfer code SKIRT (Baes et al. 2003, 2011). SKIRT is a 3D continuum radiative transfer code based on the Monte Carlo algorithm (Cashwell & Everett 1959; Witt 1977), initially developed to study the effect of dust absorption and scattering on the observed kinematics of dusty galaxies (Baes & Dejonghe 2001, 2002; Baes et al. 2003). It has been extended with a module to calculate self-consistently the dust emission spectrum under the assumption of local thermal equilibrium – LTE (Baes et al. 2005). This LTE version of SKIRT has been used to model the dust extinction and emission of galaxies and circumstellar discs (Baes et al. 2010; De Looze et al. 2010; Vidal & Baes 2007).

1.1 Dust distribution and properties

We approximated the spatial dust distribution around the primary continuum source (accretion disk) with a conical torus (i.e. a flared disc). Its characteristics are defined by (a) the half opening angle Θ – defining also the maximum height extent to which the dust is distributed –, (b) the inner and outer radius, $R_{\rm in}$ and $R_{\rm out}$ respectively, and (c) the parameters describing dust density distribution, p and q (see below). A schematic representation of the adopted geometry is given in Fig. 1. For the inner radius of the dusty torus we adopted the value of 0.5 pc, at wich the dust grains are heated to the temperature of $\sim$ 1180 K, according to the prescription given by Barvainis

(1987):

$$\left(\frac{R_{\rm in}}{\rm pc}\right) \simeq 1.3 \left(\frac{L_{\rm AGN}}{10^{46}\ {\rm erg\,s^{-1}}}\right)^{0.5} \left(\frac{T_{\rm sub}}{1500\ {\rm K}}\right)^{-2.8} \quad (1)$$

where $L_{\rm AGN}$ is the bolometric ultraviolet/optical luminosity emitted by the central source and $T_{\rm sub}$ is the sublimation temperature of the dust grains.

For the spatial distribution of the dust density we adopt a law that allows a density gradient along the radial direction and with polar angle (Granato & Danese 1994):

$$\rho\,(r,\theta) \propto r^{-p} e^{-q|cos(\theta)|}, \quad (2)$$

where r and θ are coordinates in the adopted polar coordinate system (see Fig. 1).

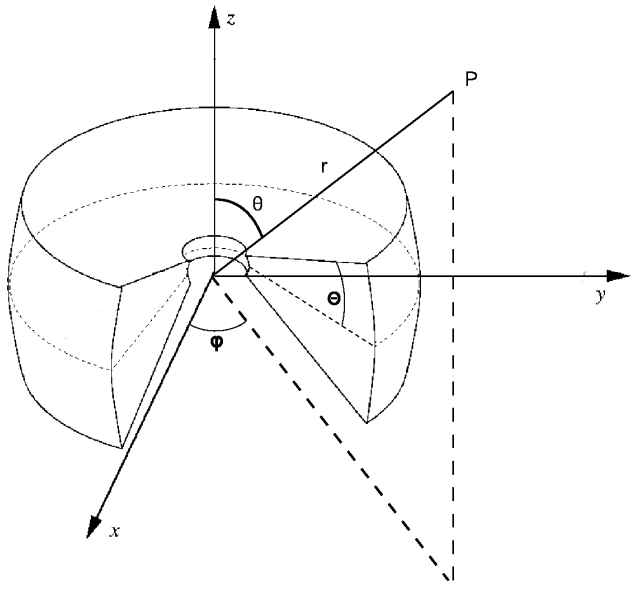

Фиг. 1. Schematic representation of the adopted model geometry and coordinate system.

The dust mixture consists of separate populations of graphite and silicate dust grains with a classical MRN size distribution (Mathis, Rumpl & Nordsieck 1977):

$$dn(a) = Ca^{-3.5}da, \quad (3)$$

where the size of grains, a, varies from 0.005 to 0.25 μm for both graphite and silicate. The normalization factors for size distribution are $C = 10^{-15.13}$ and $C = 10^{-15.11}$ for graphite and silicate, respectively (Weingartner & Draine 2001). Optical properties are taken from Laor & Draine (1993) and Li & Draine (2001).

The dust is distributed on a 3D cartesian grid composed of a large number of cubic cells. The dust density is constant within each cell. The standard resolution for our simulations is 200 cells along each axis (8×10^6 cells in total). However, to properly sample the dust properties, an increase in the torus size requires an increase of the resolution of the computational grid as well. Thus, to simulate a torus twice the size of the 'standard model', one needs to employ a grid with 400 cells along each axis, that is, 64×10^6 cells in total. To ensure that the adopted resolution is sufficient to properly sample the dust, for each simulation we compare the actual and expected values of (a) the face-on and edge-on central surface density and (b) the total dust mass.

We calculated emission for all models on an equally spaced logarithmic wavelength grid ranging from 0.001 to 1000 μm. A finer wavelength sampling was adopted between 5 and 35 μm, in order to better resolve the shape of 10 and 18 μm silicate features. Each simulation is calculated using 10^8 photon packages.

1.2 Spectral energy distribution of the primary source

The primary continuum source of dust heating is the intense UV-optical continuum coming from the accretion disc. A very good approximation of its emission is a central, point-like energy source, emitting isotropically. Its SED is very well approximated by a composition of power laws with different spectral indices in different spectral ranges. The adopted values are:

$$\lambda L_\lambda \propto \begin{cases} \lambda^{1.2} & 0.001 \leq \lambda \leq 0.01 \\ \lambda^{0} & 0.01 < \lambda \leq 0.1 \\ \lambda^{-0.5} & 0.1 < \lambda \leq 5 \\ \lambda^{-3} & 5 < \lambda \leq 50 \end{cases} \tag{4}$$

where λ is expressed in μm. These values have been quite commonly adopted in the literature, and come from both observational and theoretical arguments (see e.g., Schartmann et al. 2005). We have anyway verified that changes in the shape of the primary source SED affect only very marginally the infrared re-emission. For the bolometric luminosity of the primary source we adopted the value of 10^{11} $L_\odot$ (see e.g., Davis & Laor 2011).

1.3 Dusty torus as a clumpy two-phase medium

Models of emission in which the dust is uniformly, smoothly distributed within the toroidal region are obtained starting from Eq. 2. The density gradient is determined by the two parameters, p and q. The total amount of dust is fixed based on the equatorial optical depth at 9.7 μm ($\tau_{9.7}$). While for the smooth models distributing the dust is straightforward, for the clumpy model this process is non-trivial. As hydrodynamical simulations of Wada & Norman (2002) demonstrated, dust in tori is expected to take the form of a multiphase structure, rather than isolated clumps. Therefore, we adopted the approach which allows us to generate such a medium.

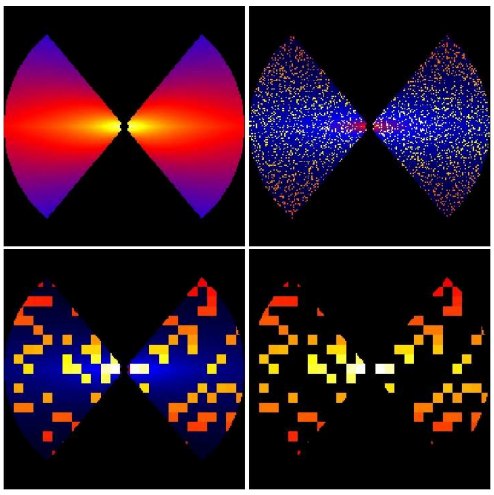

Фиг. 2. Dust density distribution at the meridional plane, given in logarithmic color scale. Density law parameters are $p = 1$ and $q = 2$. The smooth dust distribution is presented in the top left panel. The top right and bottom left panel present two-phase dust distribution for two different sizes of clumps: each clump is composed of one cubic grid cell (top right) and $8 \times 8 \times 8$ grid cells (bottom left). In the bottom right panel, a clumps-only dust distribution is presented. The contrast parameter between high- and low-density phases in the two-phase and clumps-only models is 100 and 10^9, respectively.

We start from the corresponding smooth models, i.e. the one with the same global parameters, and then apply the algorithm described by Witt & Gordon (1996) to generate a two-phase clumpy medium. According to this algorithm, each individual cell in the grid is assigned randomly to either a high- or low-density state by a Monte Carlo process. The medium created in such a way is statistically homogeneous, but clumpy. The filling factor determines the statistical frequency of the cells in the high-density state and can take values between 0 and 1. For example, a filling factor of 0.01 represents a case of rare, single high-density clumps in an extended low-density medium. The process for the clump generation is random with respect to the spatial coordinates of the individual clumps themselves. Thus, as the filling factor is allowed to increase, the likelihood that adjoining cells are occupied by clumps increases as well. This leads to the appearance of complex structures formed by several merged clumps. For filling factor values $\gtrsim 0.25$, clumps start to form an interconnected sponge-like structure, with low-density medium filling the voids. We form larger clumps by forcing high-density state into several adjoining cells.

To tune the density of the clumps and the inter-clump medium, we use the 'contrast parameter', defined as the ratio of the dust density in the high- and low-density phase. This parameter can be assigned any positive value. For example, setting the contrast to one would result in a smooth model. Setting extremely high value of contrast (> 1000) effectively puts all the dust into the clumps, without low-density medium between them. An example of

dust density distributions at the meridional plane for smooth, two-phase and clumps-only models is given in Fig. 2.

2 SKIRTOR database

SKIRTOR database can be currently reached at `https://sites.google.com/site/skirtorus/`. In this section we first present the adopted values of parameters used to calculate the available grid of models and then we provide a description of the structure of the files.

2.1 Parameter grid

For the inner and outer radius of the torus we adopted the values 0.5 and 15 pc, respectively. The half opening angle of the torus – Θ – is fixed to 50° for all of our model realizations. All models are calculated at 7 different line-of-sight inclinations, namely 0°, 40°, 50°, 60°, 70°, 80° and 90°, where $i = 0°$ represents a face-on (type 1) AGN and $i = 90°$ an edge-on (type 2) AGN. Inclinations between 0° and 40° (dust-free lines of sight) were omitted since their SED shows no appreciable difference with respect to the full face-on view. The equatorial optical depth $\tau_{9.7}$ takes values 0.1, 1.0, 5.0, 10.0. We note here that this is the optical depth of the initial smooth model, before the dust is redistributed to make the clumpy one (see Sec. 1.3). Thus, the exact value along the given line of sight will vary due to the random distribution of the clumps. The parameters defining the spatial distribution of the dust density (Eq. 2) are $p = 0$, 1 and $q = 0$, 2, 4, 6.

Defining the relative clump size, σ, as the ratio of the outer radius of the torus over the clump size:

$$\sigma = R_{out}/D_{clump} \tag{5}$$

we explored the clumpy models for two different clump sizes, 0.15 pc and 1.2 pc, that is, $\sigma = 100$ and $\sigma = 12.5$, respectively. The number of clumps in the former case is 9×10^5, and each clump occupies one grid cell. In the latter case there are ~ 3000 clumps, each one being composed of $8 \times 8 \times 8$ grid cells. The adopted filling factor values are 0.15 in the case $\sigma = 100$, and 0.25 in the case $\sigma = 12.5$ models. Both values allow us to have single, as well as clusters of high-density clumps immersed into a low-density medium. The contrast between high- and low-density phases is fixed at 100.

We generated three sets of models with the same global physical parameters: (a) models with the dust distributed smoothly, (b) models with the dust as a two-phase medium and (c) models with a contrast parameter set to an extremely high value (10^9), effectively putting all the dust into the high-density clumps. We will refer to these models as 'smooth', 'two-phase' and 'clumps-only', respectively. For clumpy models (both two-phase and clumps-only) we generated another set of models with the same parameters, but with a different random distribution of clumps.

For each model we calculated SEDs and images of torus for all the points in the wavelength grid. Calculated flux is scaled for the torus distance of 10 Mpc from the observer. The parameter grid is summarized in Table 1.

Таблица 1. The grid of parameters for which the clumps-only and two-phase models have been computed. The corresponding set of smooth models have been computed for the same parameters, except the ones which are exclusive to clumpy models only (filling factor, contrast, size of clumps)

Parameter	Adopted values
L	10^{11} $L_{\odot}$
R_{in}	0.5 pc
R_{out}	15 pc
$\tau_{9.7}$	0.1, 1.0, 5.0, 10.0
p	0, 1
q	0, 2, 4, 6
Θ	50°
Filling factor	0.15, 0.25
Contrast	100 , 10^9
Size of clumps	0.15 pc, 1.2 pc
Inclination	0°, 40°, 50°, 60°, 70°, 80°, 90°

2.2 File structure of the modeled SEDs

After the users have downloaded and unpacked the desired set of SEDs, they will have at their disposal a number of `ascii` files with their names ending with '*sed.dat'. The file names are composed of concatenated model parameters values, separated by underscores. Here are the several examples:

```
t5.0_p1_q2_oa50_2pC12_8_i0_sed.dat
t10.0_p0_q6_oa50_1pC11_1_i90_sed.dat
t1.0_p1_q0_oa50_S_8_i70_sed.dat
```

- `t` stands for $\tau_{9.7}$ (equatorial optical depth specified at 9.7 μm)
- `p`, `q` - dust density distribution parameters
- `oa` stands for half opening angle (Θ) of the torus
- `S` stands for smooth dust distribution model
- `C` stands for clumpy
- `2pC` stands for two-phase clumpy model (high density clumps with low density medium between the clumps)
- `1pC` stands for clumps-only model (without low density medium between the clumps)
- `C` is followed by a number (currently `C2`, `C11` or `C12`). This number is simply a label to distinguish different sets of models with all parameters the same, but with a different random arrangement of the clumps
- Next number (currently `1` or `8`) describes the size of clumps. `_1_` means that each clump is composed of one grid cell; `_8_` means that each clump is composed of $8 \times 8 \times 8$ cells
- `i` stands for inclination, angle between the line of sight and axis of torus, with $i = 0°$ corresponding to a face-on view and $i = 90°$ to an edge-on view.

Values of other parameters are fixed:

$L = 10^{11}\ L_{\odot}$, $R_{in} = 0.5$ pc, $R_{out} = 15$ pc $\Theta = 50°$.

Models in which each clump is composed of one grid cell (`_1_`):
Filling factor = 0.15
Total number of clumps: 9×10^5
$\sigma = R_{out}/D_{clump} = 100$; ($D_{clump} = 0.15$ pc)

Models in which each clump is composed of $8 \times 8 \times 8$ grid cells (`_8_`):
Filling factor = 0.25
Total number of clumps: ~ 3000
$\sigma = R_{out}/D_{clump} = 12.5$; ($D_{clump} = 1.2$ pc)

Two-phase models (`2pC`): Contrast = 100
Clumps-only models (`1pC`): Contrast = 10^9

Fig. 3 shows a fragment of a typical SED file. Header of a file provides a short description of what is found in each column. Here, for clarity, we provide a more detailed description of a file header:

`lambda`: wavelength (in μm.)
`Flambda`: flux at a given wavelength (in W/m^2).
`total flux`: total flux observed by a virtual instrument in a simulation.
`direct stellar flux`: remaining primary source flux that reaches the instrument (the part that is not absorbed or scattered).
`scattered stellar flux`: primary source radiation scattered at different wavelengths.
`dust flux`: flux re-emitted by the dust.
`transparent` flux: SED of the primary source.

Calculated fluxes are scaled for a source distance of 10 Mpc from the observer.

Fig. 4 shows a typical example of the total SED and its thermal and scattered components, along with the primary source emission, for the face-on and edge-on view.

2.3 Images of the dusty torus

Apart from the SEDs, we calculated images of torus for all points in the wavelength grid. These images are in the form of `fits` files and include images of total flux coming from the torus, but also separate images of the scattered, thermal, transparent and direct components. However, due to the large size of the image files, at the time being, they are available upon request. Fig. 5 shows an example of images of the torus at different wavelengths for face-on and edge-on views.

Conclusion

In this paper we presented a publicly available database of modeled SEDs of AGN dusty torus. The dusty torus was modeled as a 3D two-phase medium

```
# column 1: lambda
# column 2: lambda*Flambda (total flux)
# column 3: lambda*Flambda (direct stellar flux)
# column 4: lambda*Flambda (scattered stellar flux)
# column 5: lambda*Flambda (dust flux)
# column 6: lambda*Flambda (transparent flux)

1.00000000e-03 4.16094044e-13 4.16093004e-13 1.03997449e-18 0.00000000e+00 4.16093004e-13
1.14815362e-03 4.91125273e-13 4.91123160e-13 2.11377355e-18 0.00000000e+00 4.91123160e-13
1.31825674e-03 5.79686820e-13 5.79682799e-13 4.02123081e-18 0.00000000e+00 5.79682799e-13
1.51356125e-03 6.84218577e-13 6.84211569e-13 7.00807184e-18 0.00000000e+00 6.84211569e-13
1.73780083e-03 8.07601254e-13 8.07589037e-13 1.22165186e-17 0.00000000e+00 8.07589037e-13
...
...
...
5.75439937e+02 3.83343911e-18 0.00000000e+00 0.00000000e+00 3.83343911e-18 0.00000000e+00
6.60693448e+02 1.94115130e-18 0.00000000e+00 0.00000000e+00 1.94115130e-18 0.00000000e+00
7.58577575e+02 9.82149671e-19 0.00000000e+00 0.00000000e+00 9.82149671e-19 0.00000000e+00
8.70963590e+02 4.96446285e-19 0.00000000e+00 0.00000000e+00 4.96446285e-19 0.00000000e+00
1.00000000e+03 2.50689288e-19 0.00000000e+00 0.00000000e+00 2.50689288e-19 0.00000000e+00
```

Фиг. 3. An example of a typical SED file.

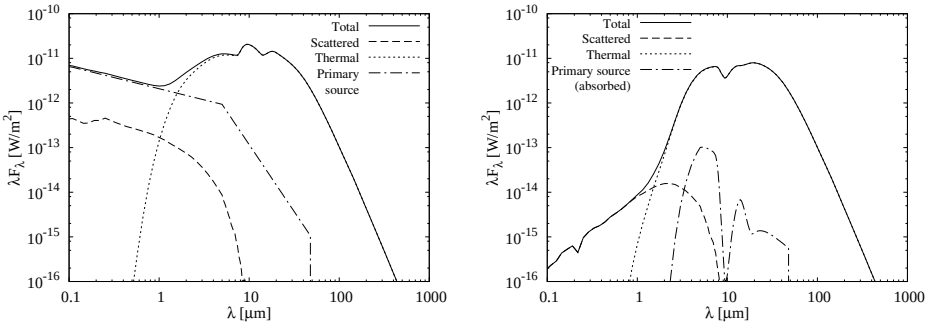

Фиг. 4. The total (solid line), thermal (dotted line), scattered (dashed line) and primary source (dash-dotted line) emission are plotted. Left panel: face-on view; right panel: edge-on view. In the face-on view, as the primary source is unobscured, the direct and transparent fluxes are identical. In the edge-on view, only the direct flux is shown.

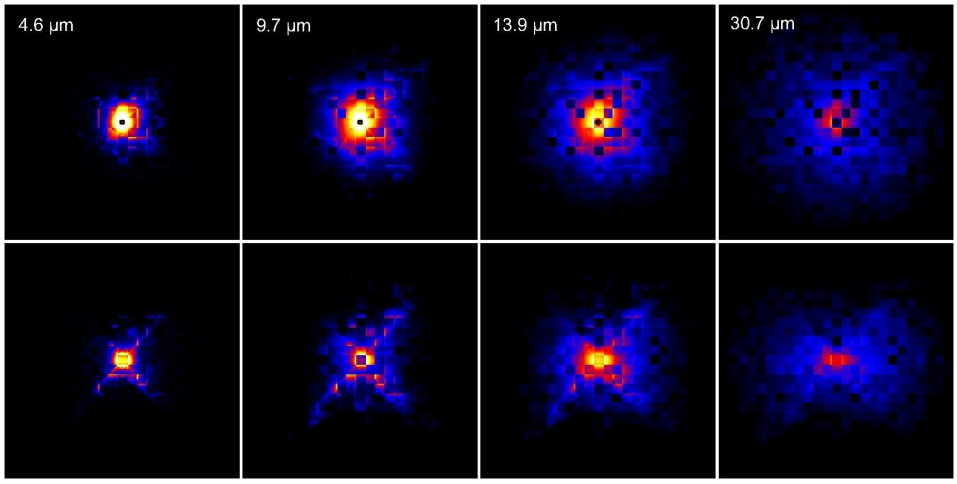

Фиг. 5. Images of the torus at different wavelengths for typical parameters of the torus. Top row is face-on view, bottom row edge-on view. From left to right, panels represent images at 4.6, 9.7, 13.9, and 30.7 μm. Images are given in logarithmic color scale. The visible squared structure is due to the clumps which in the model are in the form of cubes.

with high-density clumps and low-density medium filling the space between the clumps (Stalevski et al. 2011, 2012). This database contains a grid of models for different parameters of the torus. Also, for each two-phase model there are two corresponding models with the same global physical parameters: a clumps-only model and a model with a smooth dust distribution. Apart from the SEDs, we have calculated images of torus for all points in the wavelength grid, which are available upon request. For the convenience of potential users, here we provided a description of this database, with details on the structure of files and how to interpret them. An interested researchers may find them useful, e.g., to interpret the observed infrared properties of AGN and derive some physical and geometrical parameters. This work will be extended and the parameter grid will be progressively improved; models with different chemical composition of the dust, different torus and clumps sizes and their spatial distributions will be further explored and added to this database.

Acknowledgements

The author would like to thank Luka Č. Popović, Maarten Baes and Jacopo Fritz for very useful comments and suggestions during the construction of the database. This work was supported by the Ministry of Education, Science and Technological Development of the Republic of Serbia through the projects 'Astrophysical Spectroscopy of Extragalactic Objects' (176001) and 'Gravitation and the Large Scale Structure of the Universe' (176003).

Литература

Baes M., Davies J. I., Dejonghe H., Sabatini S., Roberts S., Evans R., Linder S. M., Smith R. M., de Blok W. J. G., 2003, MNRAS, 343, 1081
Baes M., Dejonghe H., 2001, ApJ, 563, L19
Baes M., Dejonghe H., 2002, MNRAS, 335, 441
Baes M., Dejonghe H., Davies J. I., 2005, AIPC, 761, 27
Baes M., Fritz J., Gadotti D. A., Smith D. J. B., Dunne L., da Cunha E., Amblard A., et al. 2010, A&A, 518, L39
Baes M., Verstappen J., De Looze I., Fritz J., Saftly W., Vidal Pérez E., Stalevski M., Valcke S., 2011, ApJS, 196, 22
Barvainis R., 1987, ApJ, 320, 537
Cashwell, E. D., & Everett, C. J., 1959, A Practical Manual on the Monte Carlo Method for Random Walk Problems, Pergamon, New York
Davis S. W., Laor A., 2011, ApJ, 728, 98
de Looze I., Baes M., Zibetti S., Fritz J., Cortese L., Davies J. I., Verstappen J., et al. 2010, A&A, 518, L54
Granato G. L., Danese L., 1994, MNRAS, 268, 235
Krolik J. H., Begelman M. C., 1988, ApJ, 329, 702
Laor A., Draine B. T., 1993, ApJ, 402, 441
Li A., Draine B. T., 2001, ApJ, 554, 778
Mathis J. S., Rumpl W., Nordsieck K. H., 1977, ApJ, 217, 425
Nikutta R., Elitzur M., Lacy M., 2009, ApJ, 707, 1550
Roseboom, I. G., Lawrence, A., Elvis, M., et al. 2012, submitted to MNRAS, arXiv:1205.4543
Stalevski, M., Fritz, J., Baes, M., Nakos, T., & Popović, L. Č. 2011, Baltic Astronomy, 20, 490
Stalevski, M., Fritz, J., Baes, M., Nakos, T., & Popović, L. Č. 2012, MNRAS, 420, 2756
Schartmann M., Meisenheimer K., Camenzind M., Wolf S., Henning T., 2005, A&A, 437, 861
Vidal E., Baes M., 2007, BaltA, 16, 101
Wada K., Norman C. A., 2002, ApJL, 566, L21
Wada K., Papadopoulos P. P., Spaans M., 2009, ApJ, 702, 63
Weingartner J. C., Draine B. T., 2001, ApJ, 548, 296
Witt A. N., 1977, ApJS, 35, 1
Witt A. N., Gordon K. D., 1996, ApJ, 463, 681